ACTA MECHANICA SINICA (English Series), Vol.18, No.5, October 2002 ISSN 0567-7718
The Chinese Society of Theoretical and Applied Mechanics
Chinese Journal of Mechanics Press, Beijing, China
Allerton Press, INC., New York, U.S.A.

CHARACTERIZATION OF THE FRACTURE WORK FOR DUCTILE FILM UNDERGOING THE MICRO-SCRATCH*

Wei Yueguang (魏悦广) Zhao Manhong (赵满洪) Tang Shan (唐 山)
(*LNM, Institute of Mechanics, Chinese Academy of Sciences, Beijing* 100080, *China*)

ABSTRACT: The interface adhesion strength (or interface toughness) of a thin film/substrate system is often assessed by the micro-scratch test. For a brittle film material, the interface adhesion strength is easily obtained through measuring the scratch driving forces. However, to measure the interface adhesion strength (or interface toughness) for a metal thin film material (the ductile material) by the micro-scratch test is very difficult, because intense plastic deformation is involved and the problem is a three-dimensional elastic-plastic one. In the present research, using a double-cohesive zone model, the failure characteristics of the thin film/substrate system can be described and further simulated. For a steady-state scratching process, a three-dimensional elastic-plastic finite element method based on the double cohesive zone model is developed and adopted, and the steady-state fracture work of the total system is calculated. The parameter relations between the horizontal driving forces (or energy release rate of the scratching process) and the separation strength of thin film/substrate interface, and the material shear strength, as well as the material parameters are developed. Furthermore, a scratch experiment for the Al/Si film/substrate system is carried out and the failure mechanisms are explored. Finally, the prediction results are applied to a scratch experiment for the Pt/NiO material system given in the literature.

KEY WORDS: micro-scratch test, ductile film, horizontal driving force, double cohesive zone model

1 INTRODUCTION

The micro-scratch test is an important experimental approach for determining the interfacial strength, toughness and adhesion properties for the thin film or coating layer on the substrate interface[1]. Its working principle can be described as follows. On the material or specimen surface along the vertical direction an indentation force is exerted and the indenter tip penetrates inside the material, then the indenter is moved in the horizontal and vertical directions simultaneously according to a fixed proportion. When the indenter tip moves near the film/substrate interface, a region of the thin film or coating layer near the indenter tip will be delaminated along the interface. Through measuring the driving forces, and the scratch depth, as well as the failure geometry, one may obtain the material

Received 5 November 2001, revised 14 December 2001
* The project supported by the National Natural Science Foundation of China (19891180 and 19925211) and Bai Ren Plan of CAS

or interface adhesion properties. According to usual experimental observations, there are two main kinds of failure in the scratch tests[1~9] depending on the material property of the thin film or coating, whether ductile or brittle. One kind of failure can be described as for the ductile film case, a delaminated film strap is formed before the end of the scratch test and the delaminated film strap will be curved into a circular shape. The geometry of the delaminated area is near a rectangle groove shape. Another kind of failure is for a brittle film, a fan shaped damage zone is formed near the indenter tip, inside which the film will be pressed to break up into many small pieces and also delaminated from the substrate. In the present research, our attention will be focused on the metal film/ceramic (or brittle) substrate case. The ductile failure will be simulated and analyzed in detail. Furthermore, a micro-scratch experimental research for the Al/Si system, which is extensively used in the MEMS research area, will be carried out here. The prediction results will be compared with the experimental result of a metal thin film/ceramic substrate system.

On the research of the material surface properties and adhesion work and strength of thin film or coating layer along the substrate interface, many experimental researches based on the scratch methods have been carried out in the past decade[1~9]. However, theoretical researches (or mechanics analyses) connected with the scratch experiments are very few[1]. This is because any theoretical study must deal with the complicated failure geometry of the scratch test. It is obvious that a three-dimensional elastic-plastic deformation problem must be solved, and a robust theoretical model for describing the scratch failure behavior is needed. Most theoretical researches were based on a simple geometry of the scratch failure strap and a simple mechanical equilibrium to simulate the scratch failure behavior[1~9]. However, it is difficult to use a simple model to describe the strong influence of plastic deformation on the micro-scratch behavior. It is well known that plastic deformation has a strong shielding effect on the interface cracking[10~14]. So, in an elastic-plastic failure process, more energy is dissipated than in a pure elastic failure process. Therefore, it is important to develop a reasonable mechanical model for the scratch test simulation.

On the other hand, the failure characteristics of the scratch test for ductile thin film materials[2,4,6] are somewhat similar with the thin film peeling problems. Therefore, in the micro-scratch test research, the analytical method for the thin film peeling problem[14] is relevant. It is important to obtain a reasonable relation between the critical driving force and the parameters of the materials and scratch strap geometry.

In the present research, based on the three-dimensional character of failure strap, a new mechanical model describing the interface separation and the thin film shear failure, i.e., a double cohesive zone model will be presented. Using the new model, a relation between the scratch horizontal driving force and the parameters of the materials will be set up and used to predict the scratch work. Moreover, a micro-scratch experiment for the Al/Si film/substrate system, extensively used in the MEMS research area, will be carried out. The present prediction results will be applied to a scratch experiment for the Pt/NiO material system given in the literature [6], and both results will be compared.

2 FUNDAMENTAL DESCRIPTION AND SIMPLIFICATION

From failure characteristics in ductile film scratching, the scratch test process can be described by Fig.1(a). This process comprises two stages. The first stage is a normal

scratch before thin film delamination along interface. With the indenter moving forward and downward with the increase of scratch depth, especially when the indenter tip is near the interface, a region of thin film or coating layer near the indenter tip will be delaminated from the interface. Thereby, the scratch process is transferred to another stage. The failure character changes from the indenter grooving growth to the delaminated film strap formation and growth (or post-scratch process). For simplifying the analysis, the problem is divided into two sub-problems. One problem is "plate bend" under elastic-plastic large deformation for the delaminated thin film part BCD, see Fig.1(a). This sub-problem is easy. Another problem is a three-dimensional delaminating problem for a part of thin film BA and jointed substrate. As in [14] for the peel test problem, in the present research, the solution of the former problem will be taken as the boundary condition and exerted on the section B (a small-rotation section) directly. For a mechanical analysis, usually, to set up a proper model is important[15~17]. With respect to scratch groove characters of ductile films[2,6], we present a new double-cohesive zone model to simulate the film failure and scratch work for the post-scratch process for the steady scratch advance. The model is shown in Fig.1(b). In the model, there are three cohesive zones, one is the separation-dominated cohesive zone and other two are shear-dominated cohesive zones.

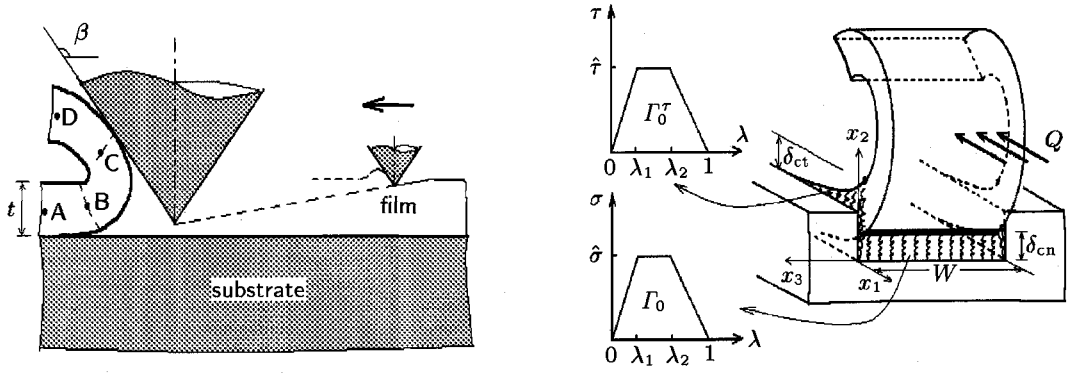

(a) (b)

Fig.1 The sketch of the micro-scratch test and the simplified model

In Fig.1(b), the thin film delaminates from the interface of thin film/substrate (plane $x_2 = 0$), and this failure process can be simulated by a separation-dominated cohesive zone surface. Simultaneously, the curved film layer is cut off from two sides of the delaminated region (planes $x_3 = -W$ and 0). The cutting process for each plane can be described by the shear-dominated cohesive zone deformation. In Fig.1(b), δ_{cn} and δ_{ct} are the critical relative displacements for the separation and shear cohesive zone surfaces, respectively. The separation cohesive zone model under plane strain case has been widely adopted and completely formulated in [10,11,13~15]. In the following, we shall discuss and give a brief description and generalization for the two kinds of cohesive zone models for the three-dimensional case.

Let $(\delta_1, \delta_2, \delta_3)$ be the relative displacements at each cohesive surface along direction (x_1, x_2, x_3), respectively, and define a normalized displacement quantity

$$\lambda = \delta_c^{-1}\sqrt{\delta_1^2 + \delta_2^2 + \delta_3^2} \tag{1}$$

The critical condition for the cohesive zone is, $\lambda = 1$. For the separation-dominated cohesive

zone case, $\delta_c = \delta_{cn}$, while for the shear-dominated cohesive zone case, $\delta_c = \delta_{ct}$. The traction relations, $\sigma(\lambda)$ and $\tau(\lambda)$, on the cohesive zone surfaces are sketched in Fig.1(b).

The tractions can be formulated in detail as follows. Define a potential function

$$\Pi(\delta_1, \delta_2, \delta_3) = \delta_{cn} \int_0^{\lambda} \sigma(\lambda') \, d\lambda' \tag{2}$$

then, the tractions can be expressed as follows

$$(T_1, T_2, T_3) = \left(\frac{\partial \Pi}{\partial \delta_1}, \frac{\partial \Pi}{\partial \delta_2}, \frac{\partial \Pi}{\partial \delta_3} \right) = \frac{\sigma(\lambda)}{\lambda \delta_{cn}} (\delta_1, \delta_2, \delta_3) \tag{3}$$

Similarly, for the shear-dominated cohesive surface, we have

$$(T_1, T_2, T_3) = \frac{\tau(\lambda)}{\lambda \delta_{ct}} (\delta_1, \delta_2, \delta_3) \tag{4}$$

Adhesion work per unit area along the cohesive surface can be written as

$$\Gamma_0 = \frac{1}{2} \hat{\sigma} \delta_{cn} (1 + \lambda_2 - \lambda_1) \tag{5}$$

for the separation zone, and

$$\Gamma_0^{\tau} = \frac{1}{2} \hat{\tau} \delta_{ct} (1 + \lambda_2 - \lambda_1) \tag{6}$$

for the shear cohesive zone. Earlier work has shown that the shape parameters (λ_1 and λ_2) of the cohesive zone model have a secondary influence on the analytical results[10,11,14]. In the present analysis, we take $(\lambda_1, \lambda_2) = (0.15, 0.5)$. Moreover, for reducing the number of governing parameters, we consider the case: $\delta_{cn} \approx \delta_{ct} = \delta_c$, thus from (5) and (6), one has $\Gamma_0^{\tau}/\Gamma_0 = \hat{\tau}/\hat{\sigma}$.

3 ENERGY BANLANCE AND ELASTIC-PLASTIC MECHANICS METHOD

The double cohesive zone model has been sketched in Fig.1(b). The variational equation for the total system based on the virtue work principle can be derived as follows

$$\begin{aligned} \int_V \delta\varepsilon_{ij}\sigma_{ij} dV &= \int_V \delta\varepsilon_{ij} D^e_{ijkl} \varepsilon^e_{kl} dV = \int_V \delta\varepsilon_{ij} D^e_{ijkl} (\varepsilon_{kl} - \varepsilon^p_{kl}) \, dV = \\ &\sum_{k=1}^{3} \left\{ \int_{S_k^+} \delta u_i t_i dS + \int_{S_k^-} \delta u_i t_i dS \right\} + WQ\delta|\Delta_1| = \\ &- \sum_{k=1}^{3} \int_{S_k} \delta|u_i^+ - u_i^-||T_i| dS + WQ\delta|\Delta_1| = \\ &- \sum_{k=1}^{3} \int_{S_k} \delta|\delta_i||T_i| dS + WQ\delta|\Delta_1| \end{aligned} \tag{7}$$

where $S_k (k = 1, 3)$ are cohesive surfaces, (u_i, t_i) are the displacement and traction components on the cohesive zone surfaces, (δ_i, T_i) are the relative displacements and tractions on the cohesive surfaces, see formulas (1) to (4). Δ_1 is the displacement of the point acted by

horizontal driving force Q per unit width, as shown in Fig.1(b). In the derivation of Eq.(7), the remote boundary conditions of the scratch test problem, which are the zero-displacement boundary condition at the bottom of the specimen and the traction-free boundary conditions at other sides, have been considered. For the curved strap, the plate-bend solution will be applied to the section B as the traction condition. Based on (7), one can develop the finite element algorithm for the scratch test problem. The incremental plastic constitutive relation is expressed as

$$\dot{\sigma}_{ij} = \frac{E}{1+\nu}\left\{\delta_{ik}\delta_{jl} + \frac{\nu}{1-2\nu}\delta_{ij}\delta_{kl} - \frac{(3/2)\,\Omega}{[1+(2/3)\,(1+\nu)\,H/E]\,\sigma_e^2}\sigma'_{ij}\sigma'_{kl}\right\}\dot{\varepsilon}_{kl} \tag{8}$$

σ'_{ij} is the deviator stress, $\sigma_e = \sqrt{3\sigma'_{ij}\sigma'_{ij}/2}$ is the effective stress; for plastic loading $\Omega = 1$, otherwise $\Omega = 0$. H is plastic modulus. In uniaxial tension, for the film material

$$\varepsilon = \sigma/E \quad \text{for} \quad \sigma < \sigma_Y \qquad\qquad \varepsilon = (\sigma_Y/E)\,(\sigma/\sigma_Y)^{1/N} \quad \text{for} \quad \sigma \geq \sigma_Y \tag{9}$$

so that

$$H = E\left\{(1/N)\,(\sigma_e/\sigma_Y)^{1/N-1} - 1\right\}^{-1} \tag{10}$$

Strap advance is assumed to occur in a steady-state such that the stress and strain increment components can be expressed as

$$(\dot{\sigma}_{ij}, \dot{\varepsilon}_{ij}) = V\,(\partial\sigma_{ij}/\partial x_1, \partial\varepsilon_{ij}/\partial x_1) \tag{11}$$

where V is the velocity of the crack tip during film delamination in x_1 direction[18]. Substituting (11) into (8), a partial differential equation in full quantities is obtained, independent of V. Plastic strain components can be expressed by the stress and total strain as

$$\varepsilon^{\mathrm{P}}_{ij} = \varepsilon_{ij} - \left(D^{\mathrm{e}}_{ijkl}\right)^{-1}\sigma_{kl} \tag{12}$$

A numerical method[19] which employs iteration to satisfy condition (11) is used to directly obtain the steady-state solution, accompanying the specially designed finite element mesh. Similarly, in the present analyses, adopting the fundamental relations of tensors and matrixes, (7) can be transformed into the finite element relations. The specially designed finite element mesh for the purposes of meeting the either steady-state growth or the boundary conditions of the three-dimensional scratch geometry as discussed above is shown in Fig.2 (half of the total mesh geometry). Note that the solution of detached film (BCD part, shown in Fig.1(a)) will be obtained separately. The element is an iso-parametric element, which includes 20 nodes. 27 Gauss integration points for each element are adopted during our numerical integration. The steps of solving the steady-state scratch problem can be described as follows: (1) Adopting a plastic strain distribution (in the first step, take $\varepsilon^{\mathrm{P}}_{ij} = 0$), find displacement and strain. (2) Find stress distributions in plastic zone and unloading zone using (8), (11) and yielding condition $\sigma_e = Y$ (Y is the current flow stress). (3) Find plastic strain by (12). Repeat those procedures until a convergent solution is obtained.

Consider that the substrate material is elastic and Young's modulus and Poisson ratio are E_s and ν_s, respectively. For a further simplification, neglect the effect of mismatch of film and substrate materials, so that we take $(E_s, \nu_s) = (E, \nu)$, furthermore, the friction between

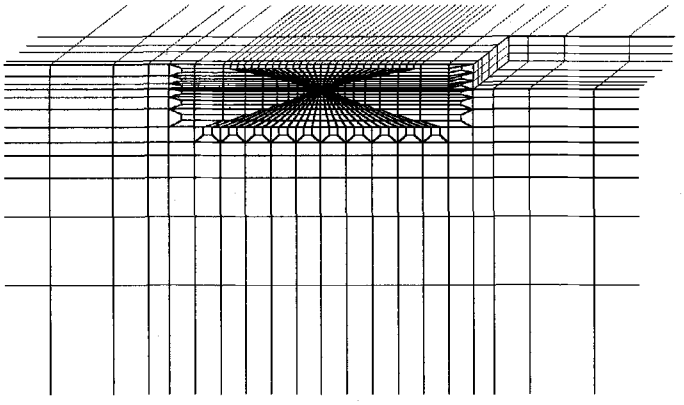

Fig.2 Three-dimensional finite element mesh for scratch geometry except for the detached film

the indenter head and the film is neglected in the present analysis. During the steady-state advance of the delaminated film strap, the total work per unit scratch advance is QW (QW is also called the energy release rate for the total system); the dissipated work per unit length along the separation cohesive surface is $\Gamma_0 W$; and along the two shear cohesive surfaces it is $2t\Gamma_0^\tau$. Let the plastic dissipation work be $W\Gamma_\mathrm{P}$. According to the energy balance under the steady-state advance, we have

$$Q = \Gamma_0 + \frac{2t}{W}\Gamma_0^\tau + \Gamma_\mathrm{P} \tag{13}$$

For elastic case, $\Gamma_\mathrm{P} = 0$. In principle, the interface separation work (interface fracture toughness) Γ_0 and the material shear work (or material shear strength) Γ_0^τ could be determined by experimental measurement. Obviously, the energy balance relation (13) for the thin film delamination based on the scratch mechanism (with part of film delamination) is different from that for the conventional thin film delamination as discussed in [13, 20]. The normalized horizontal driving force Q during the steady-state advance of failure strap can be expressed by the related independent parameters as follows

$$\frac{Q}{\Gamma_0} = 1 + \left(\frac{2t}{W}\right)\left(\frac{\hat{\tau}}{\hat{\sigma}}\right) + \frac{\Gamma_\mathrm{P}}{\Gamma_0} = f\left(\frac{E}{\sigma_Y}, \frac{\hat{\sigma}}{\sigma_Y}, \frac{\hat{\tau}}{\sigma_Y}, \frac{t}{R_0}, \frac{t}{W}, N, \nu, \beta\right) \tag{14}$$

In (14) a reference length parameter has been introduced, $R_0 = E\Gamma_0/[3\pi(1-\nu^2)\sigma_Y^2]$, characterizing the plastic zone size in the vertical direction in small scale yielding.

4 THE SOLUTION FOR DETACHED FILM STRAP

First, let us discuss the solution for the detached film strap (BCD part as shown in Fig.1(a)), which is subjected to the plastic unloading bending deformation for the steady-state scratching, as discussed in [14]. Considering the smooth contact between the indenter head and the film, the bend solution can easily be obtained as follows

$$\begin{aligned} &M = 0 \qquad \kappa = \kappa_0 \qquad \theta > \theta_\mathrm{C} = \beta \\ &M = B\kappa_0\left\{\sqrt{1 + (2Q/B\kappa_0^2 \sin\beta)\sin(\beta-\theta)} - 1\right\} \qquad \kappa = \kappa_0 + M/B \qquad \theta_\mathrm{B} < \theta \le \theta_\mathrm{C} \end{aligned} \tag{15}$$

where θ is the film slope angle with respect to x_1 direction, θ_B and θ_C are the θ values taken at section B and section C, respectively; κ_0 is the residual curvature; $B = Et^3/12(1-\nu^2)$ is the bend modulus; Q is the horizontal driving force per unit width. Other parameters are defined in Fig.1. Note that the choice of the section B location only has a small influence on the results of the total scratch problem as long as θ_B is small[14]. The residual curvature κ_0 can be calculated using the formula

$$\kappa_0 = -\frac{12}{t^3 W}\int_0^t \int_{-W}^0 \left(x_2 - \frac{1}{2}t\right)\varepsilon_{11}^{\mathrm{p}}(x_2, x_3)\,\mathrm{d}x_3\mathrm{d}x_2 \tag{16}$$

when the plastic strain component $\varepsilon_{11}^{\mathrm{p}}(x_2, x_3)$ has been obtained from the second problem, the film strap delamination problem, as discussed in the next section.

5 NUMERICAL SOLUTIONS AND ANALYSES

First apply the solution (15) to the section B (Fig.1(a)) equivalently with the linear-distributed traction, then carry out the three-dimensional finite element calculations. The finite element mesh is shown in Fig.2, and the section B is located at $x_1 = L$. The three-dimensional elastic-plastic finite element calculation for the scratch test problem is carried out based on the concepts implemented in previous sections. The results and analyses are shown in the following.

Figures 3(a)~(d) show the relations between the normalized horizontal driving force Q/Γ_0 and the maximum separation and shear strengths for two kinds of cohesive zones, scratch strap depth and width, as well as the other material parameters. Figure 3(a) shows the influences of normalized depth t/R_0 and the shear strength on the total energy release rate (the horizontal driving force). The influence of the indenter angle β on the total energy release rate is shown in Fig.3(b). Figure 3(c) shows the influence of the material yielding strength on Q/Γ_0, while Fig.3(d) shows the influence of the separation strength and the shear strength on the total energy release rate. From Figs.3(a) ~ (d), all parameters have considerably influences on the total energy release rate (the horizontal driving force). Specifically, the horizontal driving force variation is very sensitive to the shear strength and separation strength, especially for large values of the separation strength or shear strength. For the lower separation strength case, the horizontal driving force varies with the shear strength slowly as the shear strength increases, then sharply increases. For the higher separation strength, even a lower material shear strength will make the horizontal driving force increase very quickly. In Fig.3(d), the results of two different ratios, the thin film thickness to the delaminated film width, are compared. Clearly, the horizontal driving force varies sensitively with the ratios. Considering the typical metal films, in the present research, the results correspond to the lower strain hardening exponent value, i.e., $N = 0.1$. In Fig.3, the separation cohesive energy along interface Γ_0 is taken as the normalizing quantity. When the shear strength of material is zero and the elastic case is considered, the value of the normalized horizontal driving force (applied work per unit area) is equal to unity. When the material shear strength is not equal to zero, the normalized horizontal driving force will vary linearly with the shear strength from (14), for the elastic case. Obviously, from Fig.3, the energy contributed by the plastic deformation is very high.

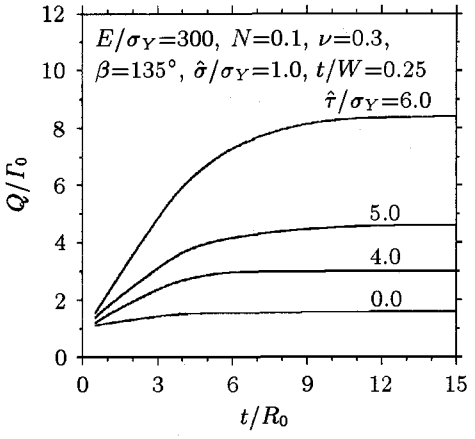

(a) With respect to the film thickness and the material shear strength

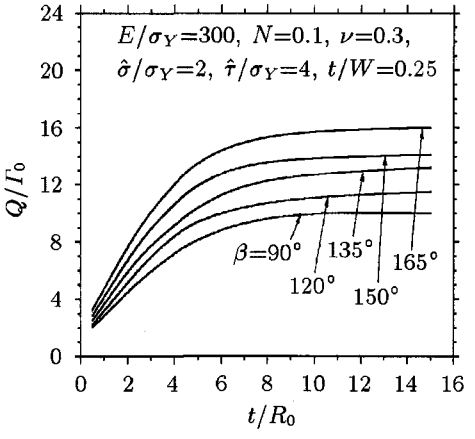

(b) With respect to the film thickness and the indenter angle

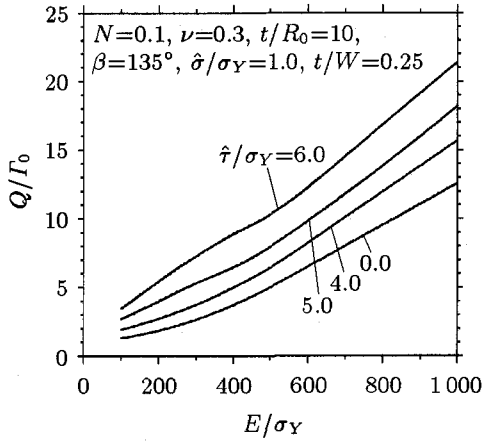

(c) With respect to the material yielding strength and shear strength

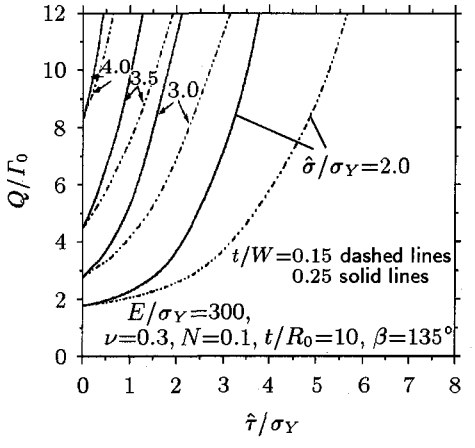

(d) With respect to the material shear strength and the interface separation strength

Fig.3 Variations of the normalized horizontal driving force (or energy release rate)

6 MICRO-SCRATCH EXPERIMENT FOR THE Al/Si SYSTEM

A micro-scratch experiment for an Al/Si film/substrate system is carried out. The specimen preparation and the experimental procedures are as follows. The specimen is prepared in the Micro-Electronic Institute of Peking University. The aluminum film is deposited on the surface of single-crystal silicon along (100) surface using the test machine Research II, the product of Sputtered Film Co., US, under the conditions of 4.6 mTorr, Ar15SCCM, and 1 000 W. The specimens for several different thicknesses of the films are considered. The micro-scratch experiments are made on the Nanoindenter II Instrument, in the State-Key Laboratory of Non-Linear Mechanics, Institute of Mechanics, Chinese Academy of Sciences. During the micro-scratch experiment, different vertical loadings within the fixed time interval (50 s) are exerted on the specimens for different film thicknesses.

Figure 4 shows the SE photographs for the specimen surface profile after the scratch experiment. Figures 5(a) and (b) show the experimental results of the total horizontal force and the vertical displacement variations with the horizontal displacement for several different thicknesses of films, respectively. From Figs.5(a) and (b), during the process of scratching, the total horizontal force increases as either the vertical or horizontal displacement increases. When the vertical displacement value approaches the film thickness, i.e. the indenter tip approaches the interface, the film is delaminated along the interface (from Fig.5(b)) abruptly. This phenomenon is similar to that of the scratch experiment for the Pt/NiO system in [6]. Thereafter, the interface crack is created and advances along the interface for a while, and soon goes down within the silicon (substrate) due to the test instrument programming automatically. The horizontal driving force increases abruptly when the indenter tip approaches the interface during scratching (Fig.5(a)), thereafter, a stable value of the horizontal force is reached with the crack advancing along the interface, soon the horizontal force increases with the indenter tip moving forward deviating inside the substrate (Fig.5(a)). Unfortunately, due to the lack of some interface parameters about the Al/Si system, such as Γ_0 value etc., the present experimental results can still not be compared with the predictions shown in the paper. The experiment work on the measurement of the adhesion energy Γ_0 for the Al/Si system is under way.

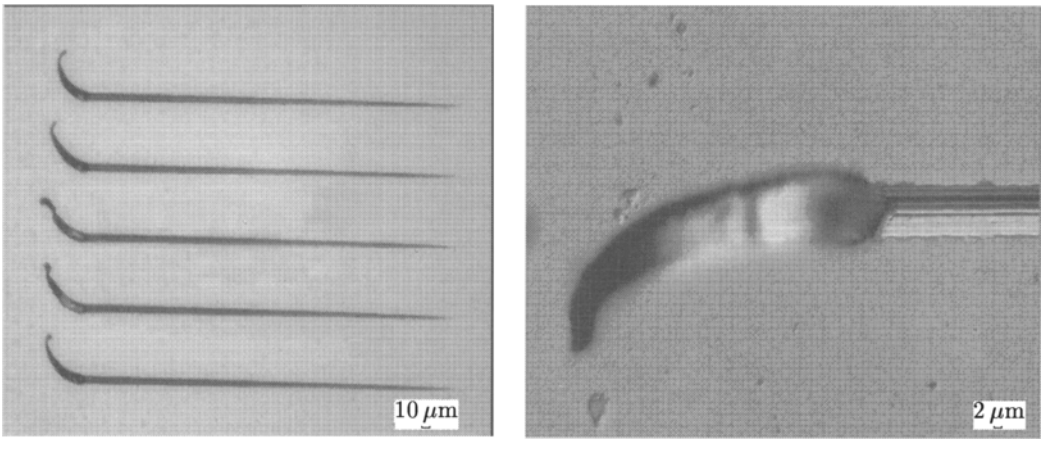

(a) A group of the scratch grooves

(b) The magnified SE photo of the scratch front profile

Fig.4 The SE photographs of the specimen surface profile

In Ref.[6], a scratch experiment for the Pt/NiO system was carried out. According to the experimental results and the related material and interface parameter values shown in [6], one can obtain $\Gamma_0 = 0.35\,\mathrm{J\cdot m^{-2}}$ and further obtain $R_0 \approx 100\,\mathrm{nm}$. The related experimental results for the scratch work and the parameters can be normalized. The normalized experimental results for the total energy release rate are plotted with the present prediction results (Fig.3(b)) together, shown in Fig.6. The prediction curves are for different indenter angles, $\beta = 90°$, $120°$, $135°$, $150°$ and $165°$. The experimental results are for the Pt/NiO film/substrate system and for the two kinds of techniques annealed at 500°C and 800°C. From Fig.6, the horizontal driving force increases as the thin film thickness increases and as the indenter angle increases. The indenter shape with the largest β corresponds to the

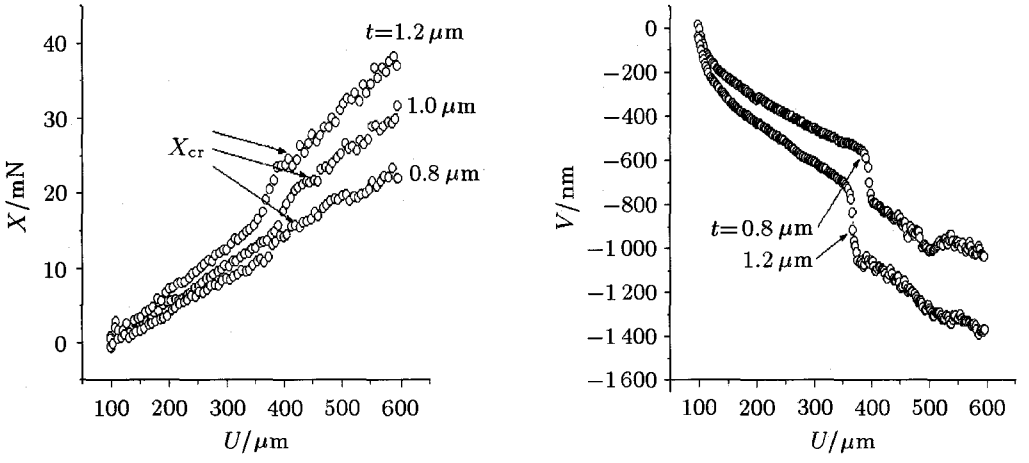

(a) The total horizontal force vs. the horizontal displacement

(b) The vertical displacement (or scratch depth) vs. the horizontal displacement

Fig.5 The micro-scratch experiment results for the Al/Si system. The experiment results of film thickness t = 0.8, 1.0 and 1.2 μm correspond to the vertical loading 70, 80 and 90 mN, respectively

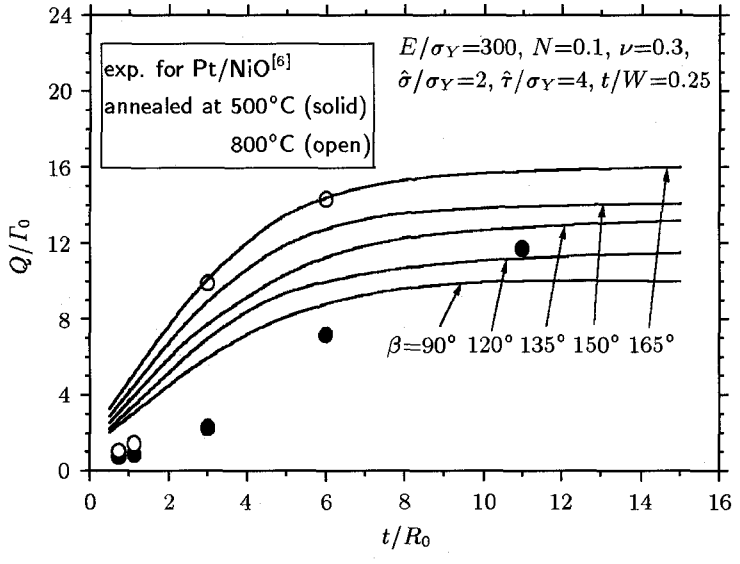

Fig.6 The comparison of the present predictions with the experimental results for the Pt/NiO system shown in [6] on the relations between the normalized horizontal driving force and the film thickness

high driving force. From Fig.6, both simulation results and experimental results show a strong work contribution from the plastic dissipation for the ductile film scratching, especially when the thin film thickness is large. As the thin film thickness increases, both results of the normalized energy release rate show a similar trend of small scale yielding.

7 CONCLUDING REMARKS

By the detailed analyses and the scratch experimental research for the Al/Si system in the present research, some important conclusions are obtained as follows: (1) Thin film plastic deformation has an important influence on the advance of delaminated film strap in the scratch test. (2) The interface separation strength and material shear strength have an important influence on the failure of thin film/substrate system. (3) The horizontal driving force depends on the thin film or coating layer thickness. With the increase of the thin film thickness, the horizontal driving force increases and approaches a stable value, which corresponds to the small scale yielding case. (4) In the micro-scratch experiment for the metal thin film on the brittle or ceramic substrate, the film delaminating mechanism shows that as the scratch front approaches the interface, the film is delaminated abruptly.

When either the interface separation strength or the material shear strength is large, a strong shielding effect from plastic deformation can be produced when the failure strengths are increased. In other words, with any cohesive strength increase, it is difficult or even impossible to make a film failure strap advance due to the strong plastic shielding. Such a prediction based on the conventional elastic-plastic theory seems somewhat contradictory to the true case. Actually, for the strong separation strength of interface or for the high shear strength, or for both, a strong plastic strain gradient effect could dominate the crack tip fields[21~24]. A reasonable simulation for this behavior might be obtained by using the strain gradient plasticity theory. A successful application of the strain gradient plasticity to the crack growth problem has been shown in [25].

On the researches of the thin film/substrate system using the scratch test methods, many experimental studies and the qualitative analyses have been presented in the past decade[1~9]. However, the analysis models based on the strict mechanics analysis have been very few[1]). This is because the scratch test problem has the obvious three-dimensional deformation characters, and a simple model will go astray from the reality[1,2,6]. In the present research, a three-dimensional analysis based on the double-cohesive zone model has been carried out for the ductile film undergoing the steady-state scratch. Adopting the strict analysis for the scratching process, although the simulation is more closer to the true scratch test case than that using a simple model, there are many parameters included in the analysis, see formula (14). Through the present research, the parameter influences on the energy release rate in the scratch test have been assessed. The detailed investigations on the importance of several dominating parameters are under way by authors.

REFERENCES

1 Blees MH, Winkelman GB, Balkenende AR, et al. The effect of friction on scratch adhesion testing: application to a sol-gel coating on polypropylene. *Thin Solid Films*, 2000, 359(1): 1~13

2 Pistor C, Friedrich K. Scratch and indentation tests on polyoxymethylene (POM). *J Appl Polymer Science*, 1997, 66(9): 1985~1996

3 Bull SJ. Failure modes in scratch adhesion testing. *Surface & Coatings Tech*, 1991, 50(1): 25~32

4 Maekawa H, Ikeda T, Horibe H, et al. On the scratch pattern of evaporated thin metal film. *Quart J Japan Welding Society*, 1994, 12(2): 262~268

5 Dutta I, Campbell JC. Determination of the adhesive strength of film-substrate interface using the constant depth scratch test. *Mater Res Soc Symp Proc*, 1995, 390(1): 49~54

6 Venkataraman S, Kohlstedt DL, Gerberich WW. Continuous microscratch measurements of the

practical and true works of adhesion for metal/ceramic systems. *J Mater Res*, 1996, 11(12): 3133~3145

7 Jardret V, Zahouani H, Loubet JL, et al. Understanding and quantification of elastic and plastic deformation during a scratch test. *Wear*, 1998, 218(1): 8~14

8 Yamamoto S, Ichimura H. Effects of intrinsic properties of TiN coating on acoustic emission behavior at scratch test. *J Mater Res*, 1992, 7(11): 2240~2247

9 Thouless MD. An analysis of spalling in the microscratch test. *Eng Frac Mech*, 1998, 61(1): 75~81

10 Tvergaard V, Hutchinson JW. The relation between crack growth resistance and fracture process parameters in elastic-plastic solids. *J Mech Phys Solids*, 1992, 40(6): 1377~1397

11 Tvergaard V, Hutchinson JW. The influence of plasticity on mixed mode interface toughness. *J Mech Phys Solids*, 1993, 41(6): 1119~1135

12 Beltz GE, Rice JR, Shih CF, et al. A self-consistent model for cleavage in the presence of plastic flow. *Acta Mater*, 1996, 44(10): 3943~3954

13 Wei Y, Hutchinson JW. Nonlinear delamination mechanics for thin films. *J Mech Phys Solids*, 1997, 45(7): 1137~1159

14 Wei Y, Hutchinson JW. Interface strength, work of adhesion and plasticity in the peel test. *Int J Fracture*, 1998, 93(1-4): 315~333

15 Needleman A. A continuum model for void nucleation by inclusion debonding. *J Applied Mechanics*, 1987, 54(3): 525~531

16 Suo Z, Shih CF, Varias AG. A theory for cleavage cracking in the presence of plastic flow. *Acta Metall Mater*, 1993, 41(5): 1551~1557

17 Wei Y, Hutchinson JW. Models of interface separation accompanied by plastic dissipation at multiple scales. *Int J Fracture*, 1999, 95(1): 1~17

18 Hutchinson JW. On steady quasi-static crack growth. Harvard University Report DEAP S-8 (AFSOR-TR-74-1042), 1974

19 Dean RH, Hutchinson JW. Quasi-static steady crack growth in small scale yielding. In: Fracture Mechanics. Philadelphia: ASTM STP700, 1980. 383~405

20 Wei Y. Microscale mechanics for metal thin film delamination along ceramic substrates. *Science in China* (Series A), 2000, 43(5): 509~516

21 Fleck NA, Hutchinson JW. Strain gradient plasticity. In: Hutchinson JW et al. eds. Advances in Applied Mechanics. New York: Academic Press, 1997, 33: 295~361

22 Gao H, Huang Y, Nix WD, et al. Mechanism-based strain gradient plasticity: I. Theory. *J Mech Phys Solids*, 1999, 47(6): 1239~1263

23 Huang Y, Gao H, Nix WD, et al. Mechanism-based strain gradient plasticity: II. Analysis. *J Mech Phys Solids*, 2000, 48(1): 99~128

24 Chen S, Wang TC. A new hardening law for strain gradient plasticity. *Acta Mater*, 2000, 48(16): 3997~4005

25 Wei Y, Hutchinson JW. Steady-state crack growth and work of fracture for solids characterized by strain gradient plasticity. *J Mech Phys Solids*, 1997, 45(8): 1253~1273